RSC Advances

PAPER

Van der Waals density functional study of the energetics of alkali metal intercalation in graphite

Cite this: *RSC Adv.*, 2014, **4**, 4069

Zhaohui Wang, Sverre M. Selbach and Tor Grande*

We report on the energetics of intercalation of lithium, sodium and potassium in graphite by density functional theory using recently developed van der Waals (vdW) density functionals. First stage intercalation compounds are well described by conventional functionals like GGA, but van der Waals functionals are crucial for higher stage intercalation compounds and graphite, where van der Waals interactions are important. The vdW-optPBE functional gave the best agreement with reported structure and energetics for graphite and LiC_6 and was further applied for intercalation of Na and K. The enthalpy of formation of LiC_6 and KC_8 were found to be −16.4 and −27.5 kJ mol^{-1} respectively. NaC_6 and NaC_8 were unstable with positive enthalpies of formation (+20.8 and +19.9 kJ mol^{-1}). The energetics of stacking of graphene and intercalant layers was investigated from first to fifth stage intercalation compounds. Higher stage compounds of Li and K were stable, but with less negative enthalpy of formation with increasing stage order. The higher stage Na compounds possessed positive enthalpy of formation, but lower in magnitude than the energy difference of 0.6 kJ mol^{-1} between graphite with AB and AA stacking. The abnormal behaviour of the lower stage Na intercalation compounds was rationalized by the lower energy involved in the formation of the chemical bond between carbon Na relative to the corresponding bond with Li or K. The chemical bond between alkali metal and carbon is characterized by charge transfer from the alkali-metal to carbon resulting in ionized alkali-metals. The intercalation induces only a subtle increase in the in-plane C–C bond lengths, with longer C–C bonds in the vicinity of the alkali metals but without breaking the hexagonal symmetry.

Received 1st December 2013
Accepted 6th December 2013

DOI: 10.1039/c3ra47187j

www.rsc.org/advances

Introduction

Graphite is a layered hexagonal material with sp^2 hybridized carbon–carbon bonds within the graphene layers and weak van der Waals (vdW) interactions between the layers.[1] Electron acceptors or donors are easily intercalated into graphite due to the weak inter-planar vdW bonds and because the intraplanar π-bands consisting of C $2p_z$ orbitals readily donates or accepts electrons. Graphite intercalation compounds (GIC) with electron donors such as alkali metals display a rich variety of phases with different compositions and crystal structures. LiC_6 and KC_8 are examples of first stage GICs with alkali metals intercalated between all the graphene layers.[1] The order of the stage refers to the number of graphene layers between two adjacent layers of intercalated alkali metal atoms. A first stage Na-GICs has never been observed, and only higher stage compounds such as NaC_{64}, where Na is only intercalated in every eighth layer, have been reported.[2]

Alkali metal GICs (AM-GICs) are important as electrodes in batteries, metallurgical processes and in molten salt electrolysis. Li-GIC has been actively investigated since the early of 1980s due to the discovery of the reversible electrochemical intercalation of lithium in graphite, which is widely used in rechargeable lithium ion batteries.[3–10] Na-GIC has drawn attention recently due to the potential as anode in a Na-ion battery as an alternative to Li-batteries.[11–15] Graphite is also used as a cathode material in electro-winning of aluminium, where sodium intercalation is known to cause chemical expansion of the cathode, change the wetting properties of the cathode and possibly influence the cathode wear.[16] Finally, K-GICs are known to be superconductors.[17]

Previous density functional theory (DFT) studies of alkali metal GICs have primarily focused on Li-GICs[18–21] and K-GICs,[22] while Na-GICs and systematic differences between Li-, Na- and K-GICs have received less attention.[23] The local density approximation (LDA) and generalized gradient approximations (GGA) have been used to study GICs, although these exchange correlation density functionals do not treat non-local van der Waals interactions properly. While GGA does not reproduce the weak interlayer interaction in graphite,[24–27] LDA can mimic a fraction of the van der Waals interactions and give a reasonable unit cell parameter *c*,[27–32] which has obscured the inability of LDA to properly account for vdW interactions.[33] With respect to energetics LDA also severely overestimates the Li–C binding energy.[34] The lack of models for vdW interactions is a fundamental limitation of traditional DFT, and much effort has been

Department of Materials Science and Engineering, Norwegian University of Science and Technology, N-7491 Trondheim, Norway. E-mail: grande@ntnu.no; Fax: +47 935 94084; Tel: +47 935 94084

devoted to solve this problem. Empirical methods based on the Lennard-Jones potential have been used to describe the structure of carbon compounds.[35–37] Semi-empirical methods based on both DFT (LDA, GGA) and empirical corrections proposed by Hasegawa *et al.*[33] and Grimme[38,39] (vdW-D) are alternative ways to describe vdW interactions. Rydberg *et al.* have constructed a tractable non-local correlation density functionals for flat surfaces and slabs[40] and applied it to graphite and other layered structures.[26,41] Langreth and Lundqvist's non-local functional (vdW-DF) was the first to be implemented in DFT.[26,42–44] The self-consistent implementation based on the algorithm of Román-Pérez and Soler[45] has been applied in studies of graphite,[46–49] K-GICs[22] and Ce-GICs.[50] Several van der Waals density functionals (vdW functionals) have recently been developed to include dispersion in DFT exchange correlation functional and implemented in VASP.[42,51,52] These functionals have been tested on cases where hydrogen bonds, dispersion bonds and mixed bonding are present with good results.[51,53] These new vdW functionals have so far not been used to study graphite intercalation compounds. A non-empirical physical treatment of the vdW interactions is necessary to compare DFT calculations on graphite and AM-GICs, and to determine the energetic stability of AM-GICs.

Here we report on a DFT study of graphite intercalation compounds with Li, K and Na by DFT functionals including weak London dispersion interactions. The recently established vdW functionals were applied to graphite and the first stage Li-GICs. The vdW-optPBE functional gave the best agreement with experimental data for graphite and LiC_6 and was used to study the energetics of Li, Na and K GICs and their polytypes from stage I to stage V. First stage Na-GICs were found to be unstable while LiC_6 and KC_8 were the most stable first stage Li- and K-GICs, respectively. Intercalation caused subtle changes in the electronic density of states and the in-plane C–C bond lengths.

Computational details

Density functional theory (DFT) calculations were performed using the VASP code,[54–58] with the five vdW functionals vdW-revPBE,[42,45] vdW-optPBE, vdW-optB88, vdW-optB86b[51] and vdW-DF2.[52] The default values of the parameters for the dW-optB88, vdW-optB86b and vdW-DF2 functionals were used in the simulations and further optimization were not carried out due to the limited amount of experimental data available. The projector augmented wave (PAW) method[59] was used with the C_h (2s, 2p), Li_sv (1s, 2s), Na_sv (2s, 2p, 3s) and K_sv (3s, 3p, 4s) potentials supplied with VASP. Electron wave functions were expanded in plane waves up to a kinetic energy cutoff of 910 eV and the SCF convergence energy was set to 10^{-7} eV. The five vdW functionals were first applied to lithium (atom and bulk), graphite (atom and bulk) and first stage Li-GICs in addition to the standard functionals GGA PBE (Perdew–Burke–Ernzerhof)[60] and LDA parameterized by Perdew and Zunger.[61] The vdW-optPBE functional was used for higher stage Li-GICs, Na, K and Na/K-GICs. The Brillouin zone was sampled with a $15 \times 15 \times 5$ Γ-centred k-point mesh for the graphite unit cell and a similar k-point density was used for all higher stage GICs. A 2nd order Methfessel–Paxton (MP)[62] smearing of $\sigma = 0.01$ eV was used for the electronic level occupancy. The convergence with respect to cutoff energy and k-point density was within 1 meV for graphite and LiC_6. Full structural relaxations of unit cell volume and atomic positions were performed until the Hellmann–Feynman forces on the ions converged to below 10^{-3} eV $Å^{-1}$. Structural relaxations of Li metal were done with all five vdW functionals, GGA and LDA with a 910 eV cutoff, a $15 \times 15 \times 15$ Monkhorst–Pack k-point mesh and the same convergence criteria as for graphite and Li-GICs. The ground state energies of C and Li atoms were calculated to obtain a reference for the cohesive energies of Li, graphite and Li-GICs. Structural relaxations of Na and K metal, and ground state energies of Na and K atoms, were done with the vdW-optPBE functional.

Results

1. Evaluation of van der Waals functionals

The five vdW functionals, vdW-revPBE, vdW-optPBE, vdW-optB88, vdW-optB86b and vdW-DF2 were evaluated by comparing the DFT results with experimental lattice parameters and cohesive energies of graphite ($P6_3/mmc$[63]) and LiC_6 ($P6/mmm$[64]), the binding energy of graphite and the enthalpy of formation of LiC_6. The enthalpy of formation is particularly important for the present aim to investigate the energetics and stability of AM-GIC polytypes. Lattice parameters, especially the long unit cell parameter c, and the binding energy gives additional insight to how well the functionals reproduce the weak inter-planar van der Waals interactions. The calculated unit cell parameters and cohesive energy (binding energy corresponding to the sublimation energy) are summarized in Tables 1 and 2. GGA did not give a stable lattice constant for the unit cell parameter c of graphite and was not reported (c increases slightly with each ionic step due to the underestimated interlayer interaction).

All functionals reproduced the experimental lattice parameter a of graphite, implying that the in-plane C–C bonds are well described. The lattice parameter c, which is perpendicular to the graphene planes and along the direction of the weak van der Waals interactions, displayed much larger deviations from the experimental value, reflecting the challenge of reproducing vdW interactions by DFT. LDA gave a small lattice parameter c and a too high cohesive energy. Compared to GGA all the five vdW functionals improve the treatment of interplanar interaction by introducing dispersion. However, vdW-optB88 and vdW-optB86b overestimate the interlayer interaction and gives a short lattice parameter c and high cohesive energy. The functionals that overestimated the interlayer interactions in graphite, like LDA, vdW-optB88 and vdW-optB86b, were disregarded as they gave even larger deviations in the lattice parameter c of LiC_6, where the Li–C interactions dominate. The calculated lattice parameter a was in excellent agreement with the experimental value for all the functionals.

For first stage GICs, like LiC_6, Li–C interactions dominate over vdW forces and the compounds are well described by the conventional GGA functional. For higher stage intercalation compounds, and in the infinite stage limit of pure graphite, vdW interactions dominate, and a suitable vdW functional

Table 1 Lattice parameters and cohesive energies E_{coh} of graphite ($P6_3/mmc$) from DFT and the deviations from experimental values. Literature values are included for comparison

	a [Å]	Δ [%]	c [Å]	Δ [%]	E_{coh} [eV per atom]	Δ [%]	Reference
LDA	2.446	−0.7	6.590	−1.80	10.10	+37.2	
GGA	—	—	—	—	—	—	
vdW-revPBE	2.476	+0.5	7.110	+5.9	8.63	+17.2	
vdW-optPBE	2.470	+0.2	6.834	+1.8	8.99	+22.0	
vdW-optB88	2.468	+0.1	6.660	−0.8	9.14	+24.1	
vdW-optB86b	2.465	0.0	6.593	−1.8	9.26	+25.6	
vdW-DF2	2.472	+0.3	6.975	+3.9	8.54	+15.9	
Exp.	2.464	—	6.711	—	7.37[a]	—	63
GGA	2.47–2.473		>7.5				22, 41, 48 and 49
LDA	2.44–2.453		6.572–6.784		7.60–9.04		30–32, 49 and 65–67
vdw-DF	2.47–2.476		6.45–7.52		8.08 (ref. 48)		22, 26, 42, 47–49 and 68

[a] At ~300 K, L. Brewer (unpublished), originally cited in ref. 28.

must be used. The vdW-optPBE and vdW-DF2 functionals performed well with respect to lattice parameters and cohesive energies of both graphite and LiC_6, while the vdW-revPBE functional gave significant deviations in the lattice parameter c of graphite.

The effect of the weak vdW interactions can also be assessed by calculating the interlayer binding energy of graphite as a function of the interlayer spacing. The calculated binding energy (corresponds to the attractive energy between graphene layers) as a function of interlayer distance with a fixed lattice constant $a = 2.46$ Å is shown in Fig. 1. The minimum binding energy defines the equilibrium interlayer distance. The functional vdW-revPBE gave the best agreement with experiments. vdW-DF2 reproduced the lattice parameters, while vdW-optPBE, vdW-optB86b and vdW-optB88 overestimated the binding energy. LDA gave a bit too low binding energy and underestimated the interplanar distance along the c-axis, while GGA could not yield a minimum in the bonding energy. PBEsol improved the treatment of interlayer interaction, but still the calculated binding energy was too low relative to experimental data.

In order to estimate the enthalpy of formation of LiC_6 the functionals were also applied to lithium metal.[74] The enthalpy of formation was then estimated from the change in cohesive energy E_{coh} for the reaction

$$\mathrm{Li(s) + 6C(graphite) = LiC_6(s)} \quad (1)$$

The internal energy of reaction (1) is estimated as

$$\Delta E_f = -(E_{coh,LiC6} - E_{coh,Li} - 6 \times E_{coh,C\ in\ graphite}) \quad (2)$$

where E_{coh} is the cohesive energy. The enthalpy of formation can be expressed as

$$\Delta H_f = \Delta E_f + pV \approx \Delta E_f \quad (3)$$

since the pV term can be neglected. The change in cohesive energy of reaction (1), corresponding to the enthalpy of formation of LiC_6 calculated by the different functionals, is summarized in Table 3.

The enthalpy of formation of LiC_6 has been reported to -13.9 ± 1.2 kJ mol^{-1}.[75] Taking into account the enthalpy of fusion of Li, which is 2.38 kJ mol^{-1} at 453.69 K,[76] the vdW-optPBE functional demonstrates the best agreement with the experimental value. LDA and vdW-DF2 overestimated the exothermic enthalpy of formation.

The preferred functional was chosen as a compromise to simultaneously describe the lattice parameters, cohesive energy and the enthalpy of reaction (1). vdW-optPBE was found as the most suitable vdW functional to describe graphite and Li-GICs as it resulted in an excellent agreement with the experimental

Table 2 Lattice parameters and cohesive energies E_{coh} of LiC_6 ($P6/mmm$) from DFT and the deviations from experimental values. Literature values are included for comparison

	a [Å]	Δ [%]	c [Å]	Δ [%]	E [eV f.u^{-1}.]	Reference
LDA	4.286	−0.1	3.536	−5.8	63.17	
GGA	4.323	+0.8	3.737	0.0	57.34	
vdW-revPBE	4.344	+1.3	3.734	−0.1	53.59	
vdW-optPBE	4.332	+1.0	3.664	−2.0	55.90	
vdW-optB88	4.328	+0.9	3.620	−3.1	56.88	
vdW-optB86b	4.322	+0.8	3.616	−3.2	57.61	
vdW-DF2	4.339	+1.1	3.730	−0.2	55.17	
Exp.	4.29	—	3.737	—		64
GGA	4.279, 4.300		3.711–3.800			19, 34 and 69
LDA	4.282, 4.300		3.690, 3.700			34, 69

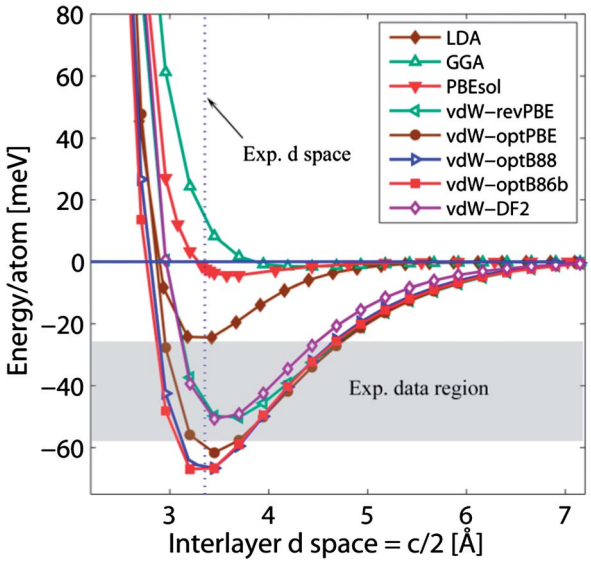

Fig. 1 Interlayer binding energy of graphite as a function of interlayer separation (d) calculated by LDA, GGA and five different vdW functionals, in all calculation lattice constant *a* was fixed as 2.46 Å. The range of experimental energies are shown as a grey region[70–73] and the experimental interlayer distance is given as the vertical line at 3.355 Å. Markers are the calculated value and lines are guides to the eye. Experimental binding energies reported shown in the figure are 31 ± 2, 43, 52 ± 5 and 35 (+15 to −10) meV per atom.[70–73]

Table 3 The calculated enthalpy of formation of LiC_6 using vdW-optPBE compared to the experimental enthalpy of formation

	ΔH [eV f.u.$^{-1}$]	ΔH [kJ mol^{-1}]	Δ [%]
LDA	−0.453	−43.7	+214
vdW-revPBE	−0.084	−8.1	−42
vdW-optPBE	−0.169	−16.3	+18
vdW-optB88	−0.231	−22.3	+60
vdW-optB86b	−0.227	−21.9	+58
vdW-DF2	−2.280	−220	+1483
Exp. 455 K (ref. 75)	—	−13.9 ± 1.2	

value of the enthalpy of formation of LiC_6 and reasonable lattice parameters and cohesive energies of graphite and LiC_6.

2. Energetics of graphite and the first stage alkali metal GICs (AM-GICs)

Graphite has three polytypes; hexagonal $P6_3/mc$, $P/6_3mmc$ and rhombohedral $R\bar{3}m$. The difference in cohesive energy of these three using the vdW-optPBE functional was less than 1 meV, which is within the convergence limit of the calculations. In the following only the $P6_3/mmc$ graphite polymorph was considered. The graphene layers in the $P6_3/mmc$ polymorph are ordered in an AB stacking sequence along the *c*-axis, while the artificial AA stacking sequence has 0.6 kJ mol^{-1} (7 meV per atom) higher energy. The equilibrium interplanar distance in graphite changes from 3.42 Å with AB stacking to 3.58 Å for AA stacking. In the first stage Li-GICs the AA stacking sequence has lower total energy than the AB, in concordance with the literature [1] as shown further below.

Polytypes of AM-GICs differ in the relative position of the alkali metal layers and the graphene layers along the long *c*-axis. The positions of the intercalants, the alkali metal atoms, on a particular site in one layer tends to exclude the placement of the intercalants on the similar sites in the nearest neighbour intercalant layer. In the nearest layer the intercalants will thus occupy equivalent intercalation sites,[1] with concomitant changes in unit cell symmetry and space group. Due to the different possible stacking sequences there is a high number of possible GICs polytypes. The different polytypes are identified by a nomenclature previously used for intercalation compounds.[1,22,69] The polytypes of LiC_6 and KC_8 considered in this work are shown in Fig. 2. LiC_6 may have the unit cell/Aα/… or /AαAβAγ/…, where A represents the graphene layer and α, β, γ represent the equivalent sites for alkali metal atoms. Correspondingly, KC_8 may have the unit cell/Aα/… or /AαAβAγAδ/…. The same considerations apply to Na-GICs, LiC_8 and KC_6, although they have not been observed experimentally.

The calculated enthalpy of formation of different polytypes of the GICs, as defined for LiC_6 by eqn (3), for Li, K and Na are shown in Fig. 3 to 5, where the crystal structures are also illustrated. Endothermic enthalpy of formation means that the compound is unstable with respect to reference state of the pure elements, while exothermic enthalpy of formation implies that the polytype structure is stable. The absolute value of the formation energy reflects the relative stability; the more negative the value the more stable the intercalation compound is with respect to the pure elements.

The most stable Li-GIC was found to be LiC_6-/Aα/, in agreement with experiments.[64] The polytype LiC_6/AαAβAγ/ has slightly higher energy than the most stable compound as illustrated in Fig 3, reflecting that it has also been observed at low temperatures.[78] The polytype LiC_6/AαBα/, which has never

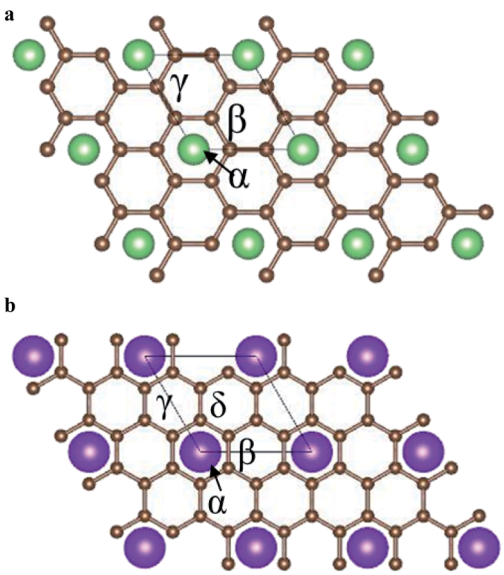

Fig. 2 MC_6 with in-plane p($\sqrt{3} \times \sqrt{3}$)R30° structure (a) and MC_8 with in-plane p(2 × 2)R0° structure (b). Carbon is represented by brown spheres, while the spheres with the other colours represent alkali metals.[77] α, β, γ and δ represent the equivalent intercalation sites.

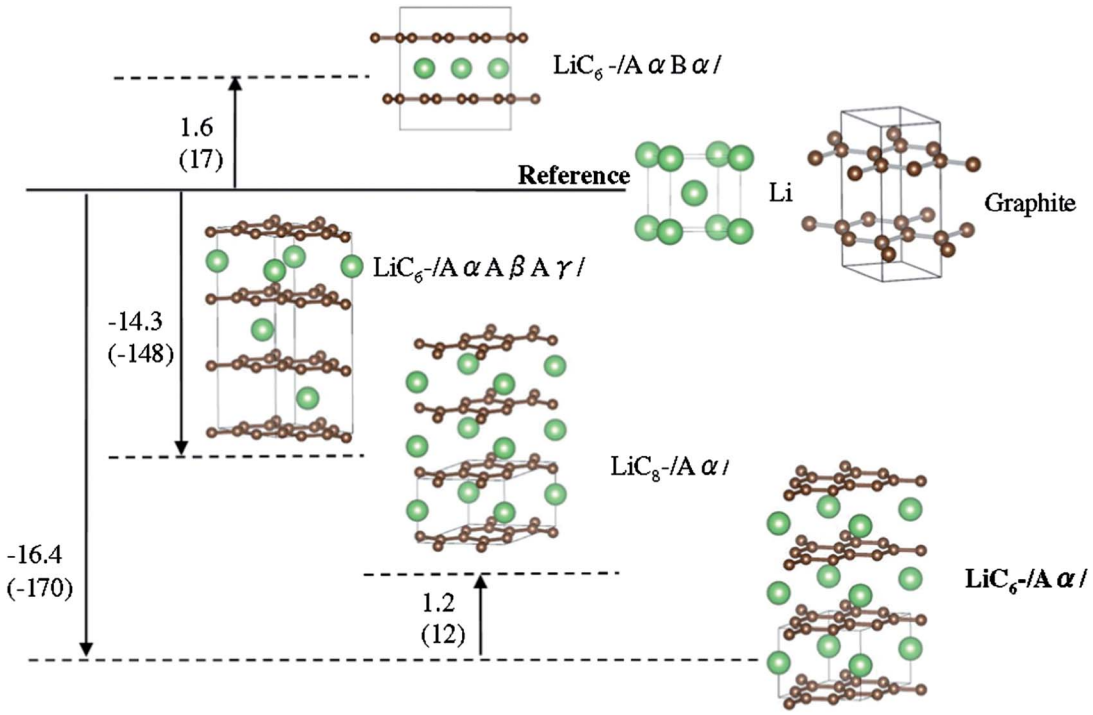

Fig. 3 Illustration of the enthalpy of formation in kJ mol^{-1} (meV f.u.$^{-1}$) of first stage Li-GICs relative to the reference state corresponding to pure graphite and Li metal. LiC_6-/Aα/ is the most stable compound. Arrow lengths are not to scale.

been reported, has higher energy than the pure substances. LiC_8-/Aα/ is also found to be less stable than LiC_6-/Aα/ (Fig. 3), following from the exothermic enthalpy of the reaction

$$LiC_8(s) = LiC_6(s) + 2C(\text{graphite}) \quad (4)$$

The calculated enthalpies of formation for K-GIC polytypes are different from the corresponding Li-GICs, as illustrated in Fig. 4. For K-GICs KC_8-/Aα/… is more stable than KC_6/Aα/…, while KC_8/AαAβAγAδ/… is found to be the most stable polytype, in concordance with experiments.[79]

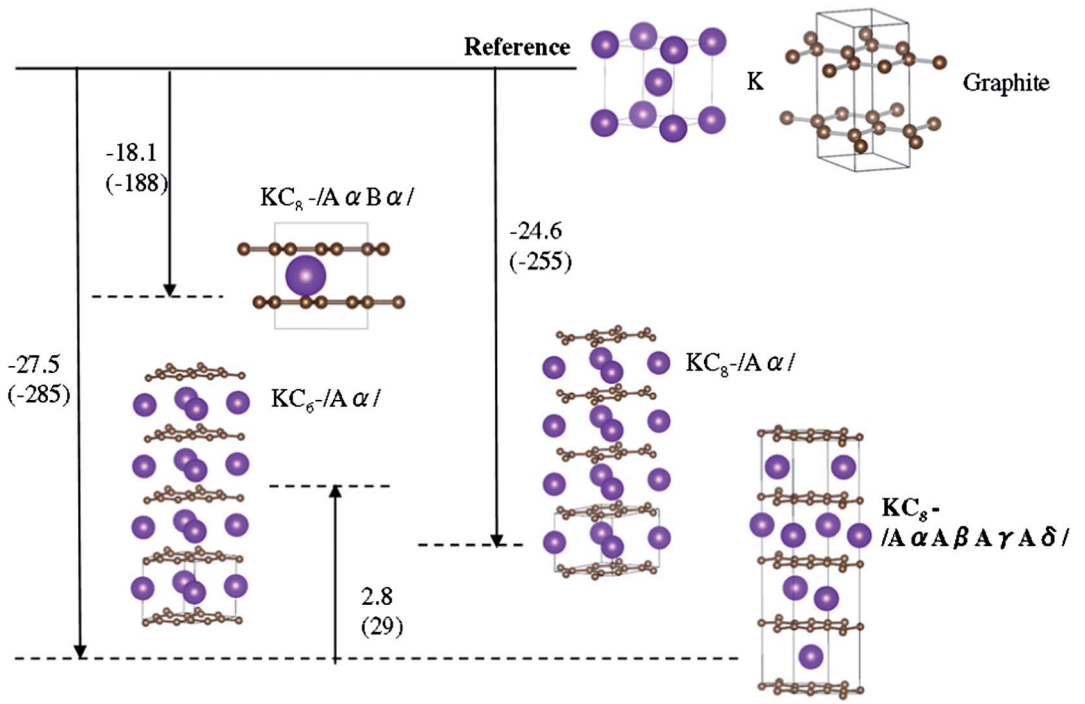

Fig. 4 Illustration of the enthalpy of formation in kJ mol^{-1} (meV f.u.$^{-1}$) of first stage K-GICs relative to the reference state corresponding to pure graphite and K metal. The compound at the lowest position is the most stable structure. Arrow lengths are not to scale.

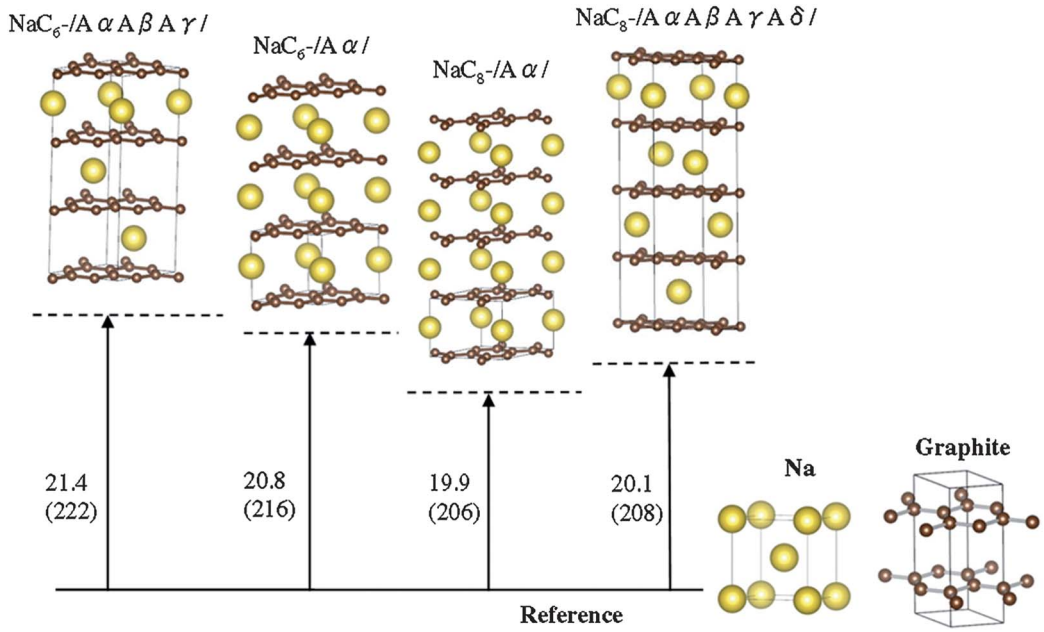

Fig. 5 Illustration of the enthalpy of formation in kJ mol^{-1} (meV f.u.$^{-1}$) of first stage Na-GICs relative to the reference state corresponding to pure graphite and Na metal. The compound at the lowest position is the most stable structure. Arrow lengths are not to scale.

The energetics of the Na-GICs polytypes (Fig. 5) is fundamentally different from the Li- and K-GICs. None of the possible first stage Na-GICs are stable with respect to the reference state of sodium metal and graphite, reflecting the lack of experimental observations of such compounds.[2]

3. Energetics of higher stage alkali metal GICs (AM-GICs)

AM-GICs form higher stage intercalation compounds with overall lower alkali content. The structure of these compounds is characterized by its stage number n which refers to the number of graphene sheets between the two nearest AM intercalant layers. The stacking sequence of the graphene layers inside the sandwich structure of higher stage AM-GICs ($n \geq 2$) has been proposed to be ABAB…,[1] corresponding to the stacking in graphite. Several polytypes of the higher stage AM-GICs are possible as in case of the first stage GIC, and we have calculated the energetic stability of the possible relevant polytypes for stage I to V GICs. Higher stage GICs were not investigated due to the computational challenges with the large unit cell and number of atoms in such systems. In an odd stage structure, the intercalant atoms in the nearest neighbour layer take the same intercalation site, while in an even stage structure, they are displaced perpendicular to the c-axis relative to the first layer. Fig. 6 illustrates a stage II and a stage III Li-GICs.

The calculated enthalpy of formation with respect to the reference state (graphite and alkali metal) is reported in Fig. 7. The enthalpy of formation per mol atom are plotted as a function of the alkali metal mole fraction in the first and higher stage Li-GICs, Na-GICs and K-GICs respectively. The compositional position of the GIC compounds is also given at the top of the figure. Dotted lines represent AM-GICs with AA graphene stacking (AM-GIC-AA) while solid lines represent AM-GICs with AB graphene stacking (AM-GIC-AB).

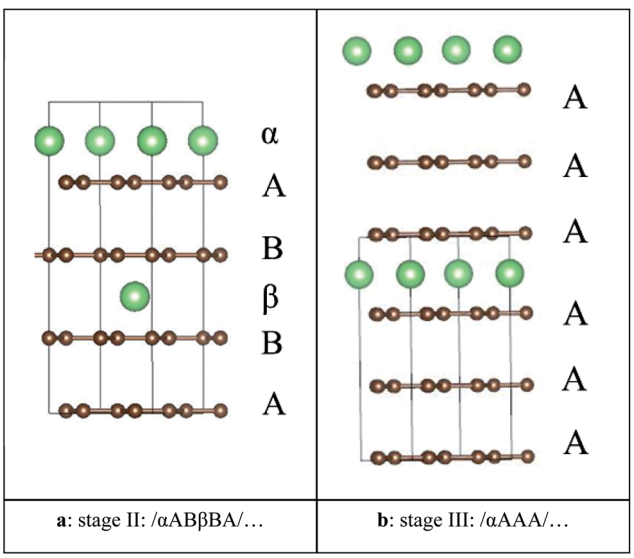

Fig. 6 Structures of stage II and III Li-GICs. Brown balls represent carbon atom and green balls represent Li metal.

We find that for stage II ($n = 2$) AM-GICs AA stacking is more stable than AB, while for $n \geq 3$, AB stacking is most stable, although the energy differences are subtle. For Li-GICs and K-GICs, all higher stage compounds were stable with respect to their neighbouring compounds, hence the energy of reaction (5) is exothermic

$$\text{GIC stage } n - 1 + \text{GIC stage } n + 1 = 2\ \text{GIC stage } n \qquad (5)$$

The stable higher stage GICs should in principle be possible to observe experimentally if the overall stoichiometry can be controlled precisely. The enthalpy of formation of Li and K GICs

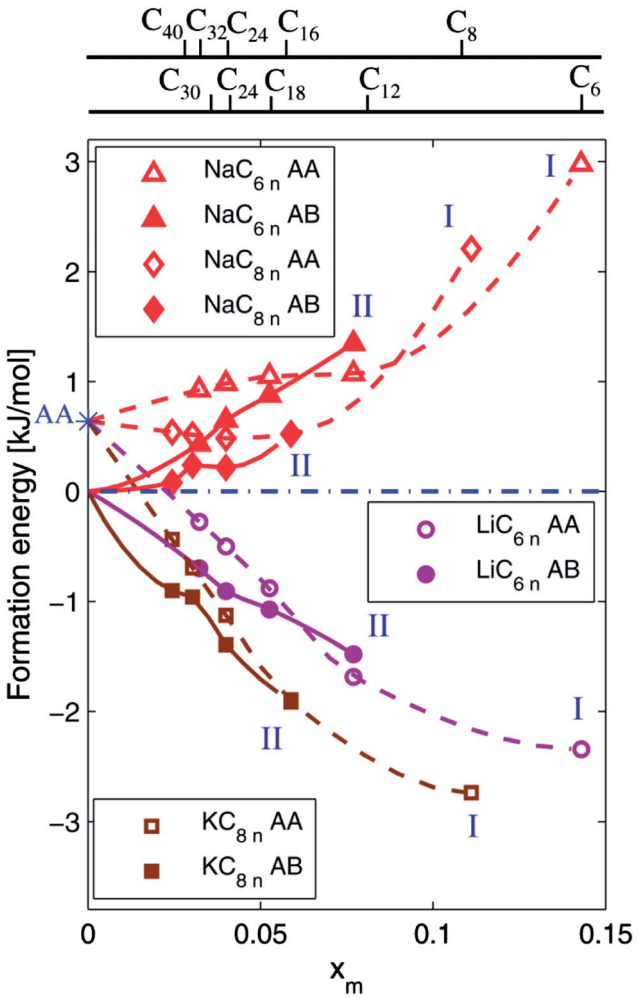

Fig. 7 The enthalpy of formation per mol atom of AM-GICs plotted as a function of composition given as the mole fraction of the alkali metal ion (x_M). The location of the different stage GICs are also given at the top of the figure. * Refer to the enthalpy of formation of artificial graphite AA compared to graphite. "I" and "II" refers to stage I and II. Dotted lines correspond to AM-GICs with AA graphene stacking (AM-GIC-AA) while solid lines correspond to AM-GICs with AB graphene stacking (AM-GIC-AB). The lines are guides to the eye.

with AB stacking sequence approach zero when $n \rightarrow \infty$ ($x_M \rightarrow 0$, which corresponds to pure graphite), while the GICs polytypes with AA stacking approach the value 0.6 kJ mol^{-1}, which is the calculated energy difference between natural AB graphite and artificial AA graphite. The energetics of Na-GICs is more sophisticated, and all the Na-GICs investigated here ($n \leq 5$) possess an endothermic enthalpy of formation, which implies that the lower stage Na-GICs is unstable in good agreement with the lack of experimental evidence for these compounds.[2,80]

Discussions

1. Crystal structure after intercalation

Intercalation of alkali metal atoms in graphite causes chemical expansion along the *c*-axis perpendicular to the graphene layers. The interlayer distance of the first stage GIC is shown in Fig. 8 together with the corresponding values for graphite with AA and AB stacking. The radii of Li, Na, K metal atoms and cations are also displayed in Fig. 8. The interlayer distances in AM-GICs clearly reflect the size of the intercalants. K^+ has by far the largest ionic radius and yields the strongest chemical expansion upon intercalation, while Li-GIC exhibit only minor chemical expansion. The expansion along the *c*-axis mainly reflects the radii of the alkali metal cations.

The in-plane C–C bond lengths in the graphene layers are also perturbed by the intercalation process. While the in-plane C–C bond lengths in pure graphite are equal, the distortion of the carbon rings by intercalation yields "long" and "short" C–C bond lengths as shown in Fig. 9. Here "L" denotes the long C–C bonds closest to the intercalants and "S" short C–C bonds further away from the intercalants. This pattern of long and short in-plane C–C bonds does not break the hexagonal symmetry of the AM-GIC. The in-plane C–C bond lengths of AB and AA graphite are included in Fig. 9 for comparison. Intercalation causes an expansion of the carbon rings, as expected from the charge transfer (see below) to the graphene layers. A larger difference between the long and short bond lengths is a possible rationalization for the lower stability of LiC_8 (NaC_8) compared to LiC_6 (NaC_6). The difference between the short and long bond lengths in K-GICs is however very small. NaC_6 differs from LiC_6 and KC_6 by displaying slightly longer C–C short and long bonds.

Further insight in the stability of the AM-GICs is provided by calculation of the artificial interlayer binding energy by fixing the lattice parameter ($a = 4.33$ Å) and variation in the interlayer distance along *c* for the first stage GICs. These calculations are performed in a similar way to the interlayer binding energy of graphite, shown in Fig. 1. The estimated interlayer binding energies of LiC_6, NaC_6 and KC_6, relative to an infinite interlayer distance, were 1.48, 0.61 and 0.86 eV f.u.$^{-1}$, respectively. NaC_6 had the lowest binding energy, which reflects the instability of

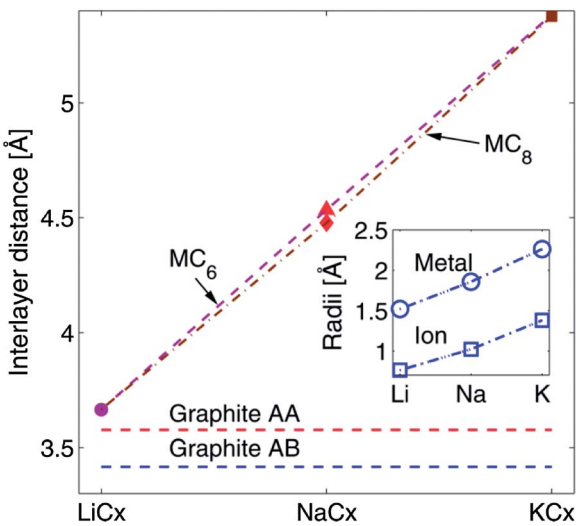

Fig. 8 The interlayer distance along the *c*-axis in AM-GICs and graphite with AB and AA stacking. Insert shows the radii of Li, Na and K (metallic radii and cation radii).[81]

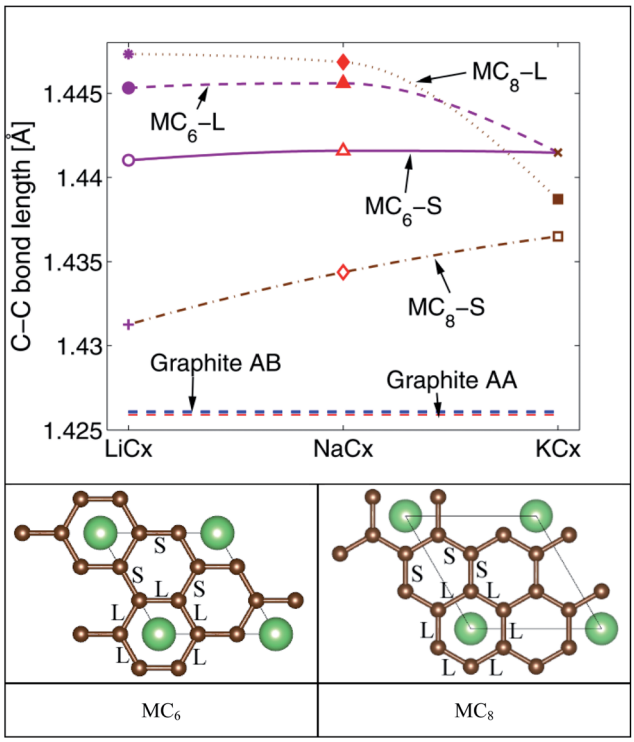

Fig. 9 [Top] In-plane C–C long (L) and short (S) bonds in MC_x intercalation compounds and graphite AB and artificial graphite AA. Configurations of long (L) and short (S) bonds for MC_6 and MC_8 are illustrated in bottom left and right figure respectively.

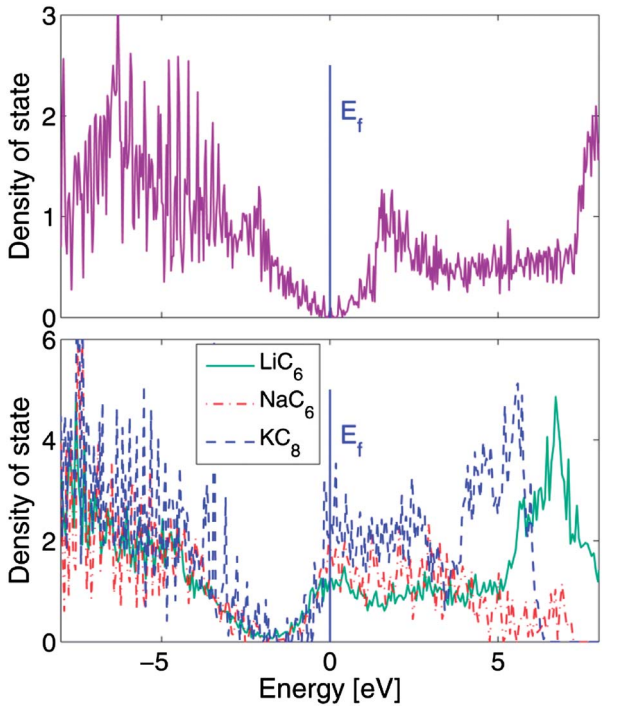

Fig. 10 Total DOS of graphite (top) and MC_x intercalation compounds (bottom).

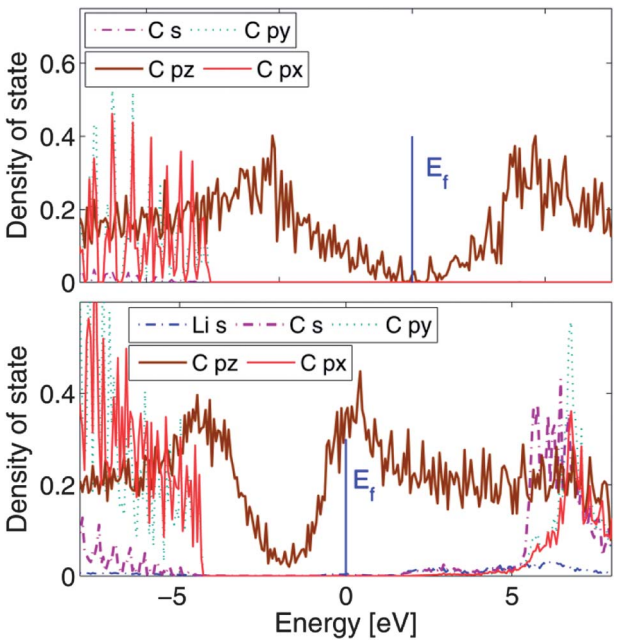

Fig. 11 Partial DOS of graphite (top) and LiC_6 (bottom).

the first stage Na-GIC and its abnormal intercalation behaviour relative to Li- and K-GICs.

2. Electronic structure after intercalation

It is also interesting to investigate the effect of electron donors like alkali metals on the electronic structure of the graphite host. The total density of state (DOS) of graphite (top) and three first stage AM-GICs (bottom) is shown in Fig. 10. While graphite is a semi-metal with close to zero band gap and negligible DOS at the Fermi energy there is a finite DOS at the E_F for the AM-GICs, which explains why the AM-GICs are metallic. All three AM-GICs have quite similar DOS in the vicinity of E_F and are expected to possess similar electronic properties, independent on the type of alkali metal. The charge densities of the three AM-GICs (not shown) are also quite similar. This reflects the strong charge transfer from the alkali metal to carbon as elucidated further below.

The partial DOS (PDOS) of graphite (top) and LiC_6 (bottom) in Fig. 11 show that only the carbon p_z orbitals contribute to the DOS at E_F. The PDOS of Na- and K-GICs are quite similar, hence only the PDOS of LiC_6 is shown. There is no overlap between Li 2s and carbon orbital energies, implying that Li completely donates its 2s electron to the carbon p_z orbitals. Integrating the PDOS of MC_x from $E_{F,graphite}$ to $E_{F,MCx}$ yields numbers very close to 1 for Li-, Na- and K-GICs investigated, implying virtually complete charge transfer from the alkali metal atoms to the carbon. These calculations demonstrate that the alkali metals become completely ionized with a formal charge of +1 as expected from the periodic table of the elements. Intercalation of the electron donors like alkali metals in carbon does therefore results in charge transfer from the donor to the carbon host in line with the expectations.

3. Abnormal behavior of Na-GICs corresponding to Li- and K-GICs

The minor difference in the electronic structures of the three AM-GICs could not explain the abnormal behavior of Na-GIC corresponding to the other two alkali metal GICs. Further insight in the abnormal behavior of Na-GICs can be obtained by de-convolution of the enthalpy of formation of GICs into several hypothetical reactions as illustrated in Fig. 12 for NaC_6. Hess law can then be applied since the internal energy is a state function. The three reaction steps are; (1) the reconstruction of the carbon host from the graphite reference state to the position of the carbon atoms in the intercalation compound, (2) reconstruction of the alkali metal from the reference bcc structure to the position of the alkali atoms in the intercalation compound, and (3) the intercalation of the hypothetical alkali layer into the carbon host. Reaction step (1) is endothermic due to the change in the stacking sequence of the graphene layers, increase in the layer spacing and finally due to elongation of the in-plane C–C bond length. The reaction step (2) is also an endothermic process due to the breaking of the metallic bond in one direction and elongation of the atomic distance to the spacing corresponding to the atomic spacing in the alkali layer in the intercalation compound. Finally, reaction step (3) is exothermic due to the charge transfer from the alkali metal to carbon and formation of the chemical bond between the two elements. The energies of the three reactions for LiC_6, NaC_6 and KC_6 are summarized in Table 4. ΔE_1 increases due to the increasing interplanar distance and increased in-plane C–C bond distance with increasing size of the alkali metal. ΔE_2 decreases due to the reducing strength of the metallic bond with increasing size of the alkali metal. Finally, ΔE_3 does not display the same dependence with the size of the alkali metal and is evidently less exothermic for NaC_6 compared to LiC_6 and KC_6, implying a lower energy gain by the charge transfer from sodium to carbon. The exothermic energy due to the charge transfer is not sufficient in order to result in an exothermic enthalpy of formation of the intercalation compound of Na.

Table 4 The enthalpy of formation and the energy of the three reactions steps, illustrated in Fig. 12, for LiC_6, NaC_6 and KC_6

	ΔE_1 [eV]	ΔE_2 [eV]	ΔE_3 [eV]	ΔH_f [eV]
LiC_6	0.101	0.657	−0.928	−0.170
NaC_6	0.236	0.278	−0.298	0.216
KC_6	0.326	0.143	−0.673	−0.204

Conclusions

Alkali metal atoms are easily intercalated in graphite due to the weak van der Waals (vdW) interactions between the graphene layers. The vdW interactions, which are not properly accounted for by conventional density functional theory (DFT), were well described by vdW-optPBE vdW exchange correlation functional. LiC_6 and KC_8 were shown to be the most stable intercalation compounds with Li and K, in agreement with experiments. In contrast, stage I to stage V Na-GICs were shown to be energetically unstable, reflecting the absence of experimental observation of lower stage Na-GICs. This instability was rationalized

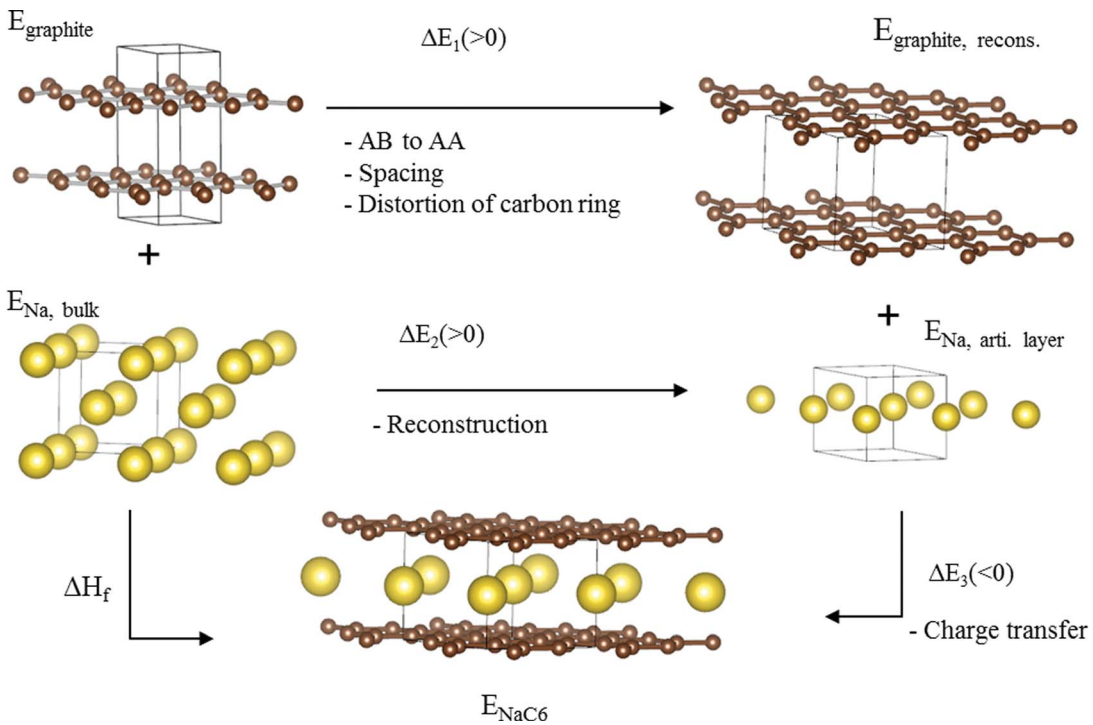

Fig. 12 The hypothetical reaction cycle for the formation of AM-GICs from the elements using NaC_6 as an example. ΔE_1 and ΔE_2 correspond to the energy required for the reconstruction of graphite and alkali metal into the layers corresponding to the intercalation compound. ΔE_3 corresponds to the energy gain from the charge transfer when the artificial alkali metal layer intercalates the carbon host.

by the low interplanar binding energy of Na-GICs. The stage I and stage II AM-GICs prefer an AA stacking sequence of the graphene layers, while in stage III and higher stage AM-GIC AB stacking of graphene layers, as in pure graphite, is the most stable configuration. The intercalation raises the Fermi energy, transforming the semi-metal graphite to metallic GICs. The chemical bonds between alkali metal atoms and carbon atoms are characterized by complete charge transfer from AM to carbon. The energy gain due to the charge transfer from Na to carbon atoms is not sufficient to cause an exothermic enthalpy of formation of the first stage GIC of Na.

Acknowledgements

The present work was carried out in the project Durable Materials in Primary Aluminium Production (DuraMat), financed by the Research Council of Norway, Hydro Aluminium, Sør-Norge Aluminium (Søral), and Elkem Carbon. Permission to publish the results is gratefully acknowledged. Computational resources were provided by NOTUR (The Norwegian Metacentre for Computational Science) through the projects nn2962k, nn9268k and nn9264k. Discussions with Gerhard Olsen concerning the abnormal behaviour of Na-GICs are acknowledged.

Notes and references

1 M. S. Dresselhaus and G. Dresselhaus, *Adv. Phys.*, 2002, **51**, 1–186.
2 R. C. Asher, *J. Inorg. Nucl. Chem.*, 1959, **10**, 238–249.
3 R. Yazami and P. Touzain, *J. Power Sources*, 1983, **9**, 365–371.
4 N. Takami, A. Satoh, M. Hara and I. Ohsaki, *J. Electrochem. Soc.*, 1995, **142**, 371–379.
5 A. Mabuchi, K. Tokumitsu, H. Fujimoto and T. Kasuh, *J. Electrochem. Soc.*, 1995, **142**, 1041–1046.
6 J. B. Goodenough, *J. Solid State Electrochem.*, 2012, **16**, 2019–2029.
7 J. S. Filhol, C. Combelles, R. Yazami and M. L. Doublet, *J. Phys. Chem. C*, 2008, **112**, 3982–3988.
8 J. Sangster, *J. Phase Equilib. Diffus.*, 2007, **28**, 561–570.
9 M. Winter, J. O. Besenhard, M. E. Spahr and P. Novak, *Adv. Mater.*, 1998, **10**, 725–763.
10 M. Endo, C. Kim, K. Nishimura, T. Fujino and K. Miyashita, *Carbon*, 2000, **38**, 183–197.
11 Y. L. Cao, L. F. Xiao, W. Wang, D. W. Choi, Z. M. Nie, J. G. Yu, L. V. Saraf, Z. G. Yang and J. Liu, *Adv. Mater.*, 2011, **23**, 3155–3160.
12 R. Alcantara, P. Lavela, G. F. Ortiz and J. L. Tirado, *Electrochem. Solid-State Lett.*, 2005, **8**, A222–A225.
13 S. W. Kim, D. H. Seo, X. H. Ma, G. Ceder and K. Kang, *Adv. Energy Mater.*, 2012, **2**, 710–721.
14 D. A. Stevens and J. R. Dahn, *J. Electrochem. Soc.*, 2000, **147**, 1271–1273.
15 M. D. Slater, D. Kim, E. Lee and C. S. Johnson, *Adv. Funct. Mater.*, 2013, **23**, 947–958.
16 K. Tschöpe, A. Støre, A. Solheim, E. Skybakmoen, T. Grande and A. P. Ratvik, *JOM*, 2013, **65**, 1403–1410.
17 R. A. Jishi and M. S. Dresselhaus, *Phys. Rev. B: Condens. Matter*, 1992, **45**, 12465–12469.
18 K. Toyoura, Y. Koyama, A. Kuwabara, F. Oba and I. Tanaka, *Phys. Rev. B: Condens. Matter Mater. Phys.*, 2008, **78**, 214303.
19 K. Persson, Y. Hinuma, Y. Meng, A. Van der Ven and G. Ceder, *Phys. Rev. B: Condens. Matter Mater. Phys.*, 2010, **82**, 125416.
20 K. Persson, V. A. Sethruaman, L. J. Hardwick, Y. Hinuma, Y. S. meng, A. v. d. Ven, V. Srinivasan, R. Kostecki and G. Ceder, *J. Phys. Chem. Lett.*, 2010, **1**, 1170–1180.
21 K. Toyoura, Y. Koyama, A. Kuwabara and I. Tanaka, *J. Phys. Chem. C*, 2010, **114**, 2375–2379.
22 E. Ziambaras, J. Kleis, E. Schroder and P. Hyldgaard, *Phys. Rev. B: Condens. Matter Mater. Phys.*, 2007, **76**, 155425.
23 S. P. Ong, V. L. Chevrier, G. Hautier, A. Jain, C. Moore, S. Kim, X. H. Ma and G. Ceder, *Energy Environ. Sci.*, 2011, **4**, 3680–3688.
24 F. Valencia, A. H. Romero, F. Ancilotto and P. L. Silvestrelli, *J. Phys. Chem. B*, 2006, **110**, 14832–14841.
25 J. I. Martínez, I. Cabria, M. J. López and J. A. Alonso, *J. Phys. Chem. C*, 2009, **113**, 939–941.
26 H. Rydberg, M. Dion, N. Jacobson, E. Schröder, P. Hyldgaard, S. I. Simak, D. C. Langreth and B. I. Lundqvist, *Phys. Rev. Lett.*, 2003, **91**, 126402.
27 G. Kern and J. Hafner, *Phys. Rev. B: Condens. Matter*, 1998, **58**, 13167–13175.
28 M. T. Yin and M. L. Cohen, *Phys. Rev. B*, 1984, **29**, 6996–6998.
29 H. J. F. Jansen and A. J. Freeman, *Phys. Rev. B*, 1987, **35**, 8207–8214.
30 M. C. Schabel and J. L. Martins, *Phys. Rev. B: Condens. Matter*, 1992, **46**, 7185–7188.
31 J. C. Boettger, *Phys. Rev. B: Condens. Matter*, 1997, **55**, 11202–11211.
32 Y. Wang, K. Scheerschmidt and U. Gösele, *Phys. Rev. B: Condens. Matter*, 2000, **61**, 12864–12870.
33 M. Hasegawa and K. Nishidate, *Phys. Rev. B: Condens. Matter Mater. Phys.*, 2004, **70**, 205431.
34 K. R. Kganyago and P. E. Ngoepe, *Phys. Rev. B: Condens. Matter*, 2003, **68**, 205111.
35 L. A. Girifalco and M. Hodak, *Phys. Rev. B: Condens. Matter*, 2002, **65**, 125404.
36 L. A. Girifalco, M. Hodak and R. S. Lee, *Phys. Rev. B: Condens. Matter*, 2000, **62**, 13104–13110.
37 H. Ulbricht, G. Moos and T. Hertel, *Phys. Rev. Lett.*, 2003, **90**, 095501.
38 S. Grimme, *J. Comput. Chem.*, 2004, **25**, 1463–1473.
39 S. Grimme, *J. Comput. Chem.*, 2006, **27**, 1787–1799.
40 H. Rydberg, B. I. Lundqvist, D. C. Langreth and M. Dion, *Phys. Rev. B: Condens. Matter*, 2000, **62**, 6997–7006.
41 H. Rydberg, N. Jacobson, P. Hyldgaard, S. I. Simak, B. I. Lundqvist and D. C. Langreth, *Surf. Sci.*, 2003, **532–535**, 606–610.
42 M. Dion, H. Rydberg, E. Schröder, D. C. Langreth and B. I. Lundqvist, *Phys. Rev. Lett.*, 2004, **92**, 246401.
43 M. Dion, H. Rydberg, E. Schröder, D. C. Langreth and B. I. Lundqvist, *Phys. Rev. Lett.*, 2005, **95**, 109902.

44 D. C. Langreth, M. Dion, H. Rydberg, E. Schröder, P. Hyldgaard and B. I. Lundqvist, *Int. J. Quantum Chem.*, 2005, **101**, 599–610.
45 G. Román-Pérez and J. M. Soler, *Phys. Rev. Lett.*, 2009, **103**, 096102.
46 P. Lazić, N. Atodiresei, V. Caciuc, R. Brako, B. Gumhalter and S. Blügel, *J. Phys.: Condens. Matter*, 2012, **24**, 424215.
47 S. Lebègue, J. Harl, T. Gould, J. G. Ángyán, G. Kresse and J. F. Dobson, *Phys. Rev. Lett.*, 2010, **105**, 196401.
48 Y. Ma, *Phys. Rev. B: Condens. Matter Mater. Phys.*, 2007, **76**, 075419.
49 I. Hamada and M. Otani, *Phys. Rev. B: Condens. Matter Mater. Phys.*, 2010, **82**, 153412.
50 M. Büttner, P. Choudhury, J. Karl Johnson and J. T. Yates Jr, *Carbon*, 2011, **49**, 3937–3952.
51 J. Klimeš, D. R. Bowler and A. Michaelides, *J. Phys.: Condens. Matter*, 2010, **22**, 074203.
52 K. Lee, É. D. Murray, L. Kong, B. I. Lundqvist and D. C. Langreth, *Phys. Rev. B: Condens. Matter Mater. Phys.*, 2010, **82**, 081101.
53 J. Klimeš, D. R. Bowler and A. Michaelides, *Phys. Rev. B: Condens. Matter Mater. Phys.*, 2011, **83**, 195131.
54 P. E. Blöchl, *Phys. Rev. B: Condens. Matter*, 1994, **50**, 17953–17979.
55 G. Kresse and J. Hafner, *Phys. Rev. B: Condens. Matter*, 1993, **47**, 558–561.
56 G. Kresse and J. Hafner, *Phys. Rev. B: Condens. Matter*, 1994, **49**, 14251–14269.
57 G. Kresse and J. Furthmüller, *Comput. Mater. Sci.*, 1996, **6**, 15–50.
58 G. Kresse and J. Furthmüller, *Phys. Rev. B: Condens. Matter*, 1996, **54**, 11169–11186.
59 G. Kresse and D. Joubert, *Phys. Rev. B: Condens. Matter Mater. Phys.*, 1999, **59**, 18.
60 J. P. Perdew, K. Burke and M. Ernzerhof, *Phys. Rev. Lett.*, 1996, **77**, 3865–3868.
61 J. P. Perdew and A. Zunger, *Phys. Rev. B*, 1981, **23**, 5048–5079.
62 M. Methfessel and A. T. Paxton, *Phys. Rev. B*, 1989, **40**, 3616–3621.
63 P. Trucano and R. Chen, *Nature*, 1975, **258**, 136–137.
64 R. Juza and V. Wehle, *Naturwissenschaften*, 1965, **52**, 560–560.
65 J. Furthmüller, J. Hafner and G. Kresse, *Phys. Rev. B: Condens. Matter*, 1994, **50**, 15606–15622.
66 B. I. Dunlap and J. C. Boettger, *J. Phys. B: At., Mol. Opt. Phys.*, 1996, **29**, L7.
67 S. B. Trickey, F. Müller-Plathe, G. H. F. Diercksen and J. C. Boettger, *Phys. Rev. B: Condens. Matter*, 1992, **45**, 9.
68 S. D. Chakarova-Käck, E. Schröder, B. I. Lundqvist and D. C. Langreth, *Phys. Rev. Lett.*, 2006, **96**, 146107.
69 Y. Imai and A. Watanabe, *J. Alloys Compd.*, 2007, **439**, 258–267.
70 Z. Liu, J. Z. Liu, Y. Cheng, Z. Li, L. Wang and Q. Zheng, *Phys. Rev. B: Condens. Matter Mater. Phys.*, 2012, **85**, 205418.
71 R. Zacharia, H. Ulbricht and T. Hertel, *Phys. Rev. B: Condens. Matter Mater. Phys.*, 2004, **69**, 155406.
72 N. G. C, L. X. Benedict, M. L. Cohen, A. Zettl, S. G. Louie and V. H. Crespi, *Chem. Phys. Lett.*, 1998, **7**, 490–496.
73 L. A. Girifalco and R. A. Lad, *J. Chem. Phys.*, 1956, **25**, 5.
74 S. H. Kellington, D. Loveridge and J. M. Titman, *J. Phys. D: Appl. Phys.*, 1969, **2**, 1162–1163.
75 V. V. Avdeev, A. P. Savchenkova, L. A. Monyakina, I. V. Nikol'skaya and A. V. Khvostov, *J. Phys. Chem. Solids*, 1996, **57**, 947–949.
76 D. R. Stull, JANAF Thermochemical Tables, in *The Thermal Research Laboratory*, Dow Chemical Company, Michigan, USA, 1965.
77 K. Momma and F. Izumi, *J. Appl. Crystallogr.*, 2008, **41**, 653–658.
78 N. Kambe, M. S. Dresselhaus, S. Basu, A. R. McGhie and J. E. Fischer, *Mater. Sci. Eng.*, 1979, **40**, 1–4.
79 P. Lagrange, D. Guerard and A. Herold, *Annales de Chimie Science des Matériaux*, 1978, **3**, 143–159.
80 J. Sangster, *J. Phase Equilib. Diffus.*, 2007, **28**, 571–579.
81 R. Shannon, *Acta Crystallogr., Sect. A: Cryst. Phys., Diffr., Theor. Gen. Crystallogr.*, 1976, **32**, 751–767.